Romanian Reports in Physics, Vol. 67, No. 4, P. 1346–1358, 2015

Dedicated to
International Year of Light 2015

HANDHELD SCANNING PROBES FOR OPTICAL COHERENCE TOMOGRAPHY

V.-F. DUMA[1, 2, 3], G. DOBRE[4], D. DEMIAN[1], R. CERNAT[4], C. SINESCU[5], F.I. TOPALA[5], M.L. NEGRUTIU[5], G. HUTIU[1], A. BRADU[4], A.G. PODOLEANU[4]

[1]Aurel Vlaicu University of Arad, 3OM Optomechatronics Group, 77 Revolutiei Ave., Arad 310130, Romania, E-mail: duma.virgil@osamember.org
[2]Doctoral School, Polytechnics University of Timisoara, 1 Mihai Viteazu Ave., Timisoara 300222, Romania
[3]Faculty of Physics, West University of Timisoara, 4 Vasile Parvan Ave., Timisoara 300223, Romania
[4]University of Kent, Applied Optics Group, School of Physical Sciences, Canterbury, CT2 7NH, UK, E-mail: gd@kent.ac.uk
[5]"Victor Babes" Medicine and Pharmacy University of Timisoara, Faculty of Dental Medicine, 2A Eftimie Murgu Place, 300070 Timisoara, Romania

Received August 27, 2015

Abstract. We report the design of two handheld scanning probes for Optical Coherence Tomography (OCT). The probes are equipped with a one-dimensional (1D) galvanometer scanner (GS), offering cross-sectional capabilities with OCT. One of the variants of the probe is tested in the lab, including *in vivo* on healthy volunteers.

Key words: Biomedical imaging, Optical Coherence Tomography (OCT), handheld probes, galvanometer scanners, optomechanical design, testing, skin, dentistry.

1. INTRODUCTION

Optical Coherence Tomography (OCT) is a biomedical imaging technique, which is based on the principle of low coherence interferometry [1–3]. Its development started in the early 1990s with studies of the low coherence imaging of layers in the retina of the human eye [1], and has progressively expanded to imaging the anterior segment of the eye [4], skin [5], teeth [6–8] and oral mucosa [9], as well as various lumens of the body by using endoscopic techniques [10].

Various aspects of OCT performance have improved over the last two decades. Depth, or axial resolution, has improved from the original 15–20 μm [1] to 3–5 μm (commonly achieved) and some groups have pushed that boundary further to around 1 μm [11]. Imaging speed went from 2 planar frames per second [1] to 45 GVoxels per second, which leads to the capability of imaging a volume of tissue in a fraction of a second [12].

Other parameters such as penetration depth depend on the properties of the tissue or the material investigated, therefore they are more related to the specific application targeted.

This progress has been linked to the development of several broadly defined techniques, from the initial Time-Domain (TD) OCT (broad spectrum used for illumination, signal obtained at a photodetector by scanning the length of the reference arm) to Spectral Domain (SD) OCT (with no moving arms and a broad spectrum of interference detected with a spectrometer) and to Swept Source (SS) OCT (with no moving arms, a narrow spectral line swept over a range of wavelengths, and with signal obtained at a photodetector) [13, 14].

In order to improve its investigation capabilities, OCT is also being used in conjunction with other techniques such as confocal microscopy or scanning laser ophthalmoscopy [15, 16]. The increased speed and noise performance of techniques like SD and SS OCT allow current acquisition of many volumes of data per second, which is necessary for *in vivo* investigations of biological tissue.

The vast majority of studies on OCT have reported improvements of the OCT engine but did not deal closely with the way in which light is delivered to tissue, particularly for non-ophthalmic applications. In order to move the technique from the lab to the clinic and apply it on patients, the OCT system should be engineered as a mobile unit and equipped with handheld probes, in order to be able to point at a specific area of interest on the patient's body. The present work is part of this significant effort which is being made in that direction, for OCT [17, 18], as well as for other biomedical imaging techniques [19, 20].

Such systems also have the specificity of targeting a range of applications, either *ex vivo* or *in vivo* from accessible surface skin and mucosal lesions on the scalp, face, neck and oral cavity, for example in an Ear, Nose and Throat (ENT) department, as performed at the Northwick Park Hospital (part of London North West Healthcare NHS Trust, London, UK) [21] or in a primary care unit – with a range of investigation capabilities, *e.g.* for the eye or ear, in order to further the diagnostic capabilities of otoscopes and ophthalmoscopes [22].

The OCT handheld probes must have an appropriate design and adapters to allow for these goals. Their level of complexity must also be correlated with the specific applications targeted. Previous designs have employed bi-dimensional (2D) scanning systems in the probes [23, 24]: dual axis galvanometer-based scanners (GSs) [22] or Micro-Electro-Mechanical Systems (MEMS) [25]. Such scanning heads provide 3D/volumetric OCT reconstructions of the samples investigated, as required for example in ophthalmoscopy. Other areas of biomedical imaging in clinic such as dental medicine are satisfied with the cross-sectional capabilities of the OCT system, as we have recently demonstrated *ex vivo* for the monitoring of dental procedures (*i.e.* drilling) on teeth [7] or, for the final investigations, for the interface between sealant and tooth [8].

As we have also shown in numerous reports [7–9, 26], OCT offers in dentistry imaging capabilities that are necessary and that are not offered by current established investigation techniques. Visual inspection or classical microscopy for example cannot show defects beneath the surface, while the assessment is difficult

and subjective, depending on the dentist's experience [8]. Radiography can be applied only before or after dental procedures and carries a radiation exposure hazard. In contrast, OCT is non-invasive and it can also be applied in real time, for example during the time that dental work is carried out [7].

The 1-D GS handheld probes we designed, built and tested are appropriate in the context described above, and have found an immediate use in the dental clinic: they provide transversal depth sections (termed B-scans in OCT) in the tissue investigated, as we previously demonstrated *ex vivo* for metalloceramic prostheses [27] or *in vivo* for ENT [21].

In this report we present two of the probe designs we developed, coupled with an SS-OCT platform also built in our groups, as well as testing of such probes for imaging a range of samples, including *in vivo* on healthy volunteers.

2. OCT METHOD AND SETUP

The OCT engine developed and built in-house has at its core a 50 kHz laser swept source (Axsun Technologies Ltd) centred at 1310 nm, with a sweeping range between 1256.6 nm–1362.8 nm (Fig. 1). The output optical power of 18 mW is directed into a Wavelength Division Multiplexer (WDM) where it is combined with 633 nm light (whose purpose is to provide aiming guidance on the sample).

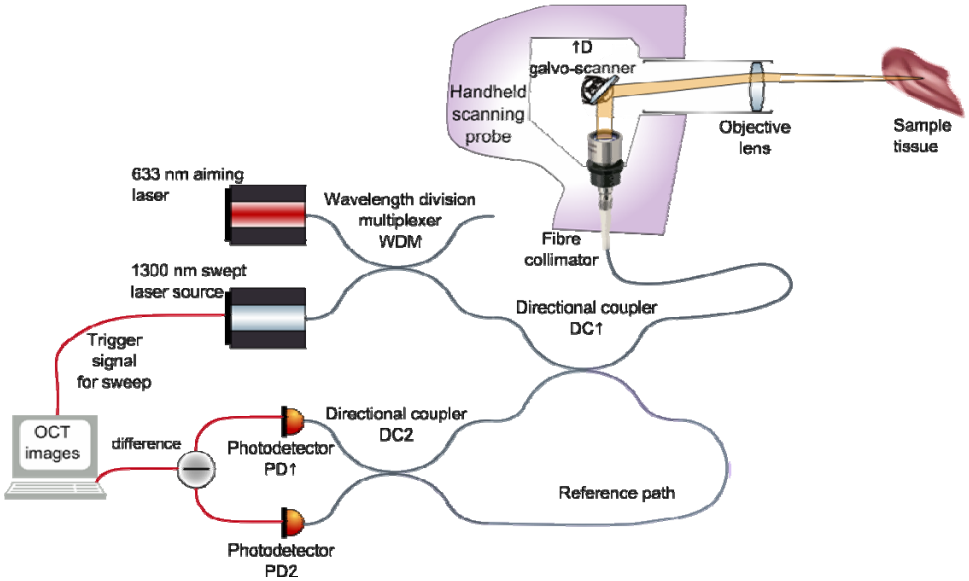

Fig. 1 – Schematic diagram of the in-house developed SS-OCT system.

The use of an 80/20 directional coupler ensures that 20% of the source power reaches the fibre collimator at the handheld probe input and 80% of the backreflected light from the sample is guided back through the handheld probe along the same path and subsequently combined at coupler DC2 with the reference light (which carries the remaining 80% of the source power and travels along the reference path, identified in the diagram). Each of the two DC2 arms leading to photodetectors carries interference light resulting from the recombination of sample and reference light, and due to the properties of directional fibre couplers these two interference signals at the output of DC2 are of opposite phase. They are converted into two electronic signals (also of opposite phase) at the differential detection system consisting of two photodetectors (PD1 and PD2, Santec Model BPD-200 DC).

The signal resulting from the difference operation is stripped of its DC slow varying component and is left with twice the amplitude of the interference between sample and reference beams.

This signal is further digitised by a 12-bit, 500 MS/s waveform digitizer (Alazar ATS9350), converted to greyscale, put in a form suitable for viewing, and displayed using Labview software developed in-house.

The schematic of the handheld probe (several variants of which have been developed) is also shown in Fig. 1 directing the beam to the sample tissue. Its structure can be correlated with the optomechanics presented in Fig. 2: it comprises an ergonomic handle housing the fibre collimator and a heatsink assembly in which the GS is mounted. The objective lens has 30 mm focal length.

3. HANDHELD SCANNING PROBE FOR OCT – WITH A SINGLE AXIS GALVANOMETER SCANNER

Several designs of such OCT probes were developed [27], from variants built almost entirely from off-the-shelf components – as shown in the example in Fig. 2a – to an ergonomic configuration which uses the same key components (*i.e.*, fibre collimator, 1D GS, and lens), but includes them in a setup that has been designed to be more sturdy, simple, and light weight (Fig. 2b,c).

Details of the specific Thorlabs components we have utilized in our probes have been provided in [27], including their codes, weights, and costs. Thus, the weight of our handheld probes ranged from 0.25 kg to 0.33 kg – in comparison with probes built with MEMS (which are from the start much lighter than GSs), which reached a minimum of 0.5 kg [25], while commercially available probes (which do include a significant part of the OCT system) go up to 2.2 kg, like iVue (Optovue, Fremont, CA, USA) [28]; for the latter, the probes are not even held in the hand, but placed on supports in order to be used.

Also, the added cost of our probes is around 150 euro – both for the initial variant in Fig. 2a and for the final, ergonomic probe in Fig. 2b; this cost does not include the three key components mentioned above, but these must be part of any

bench-mounted OCT setup anyway. Essentially, our construction takes these components from the bench setup and couples them in a device that can be placed in a convenient way around the patient's body.

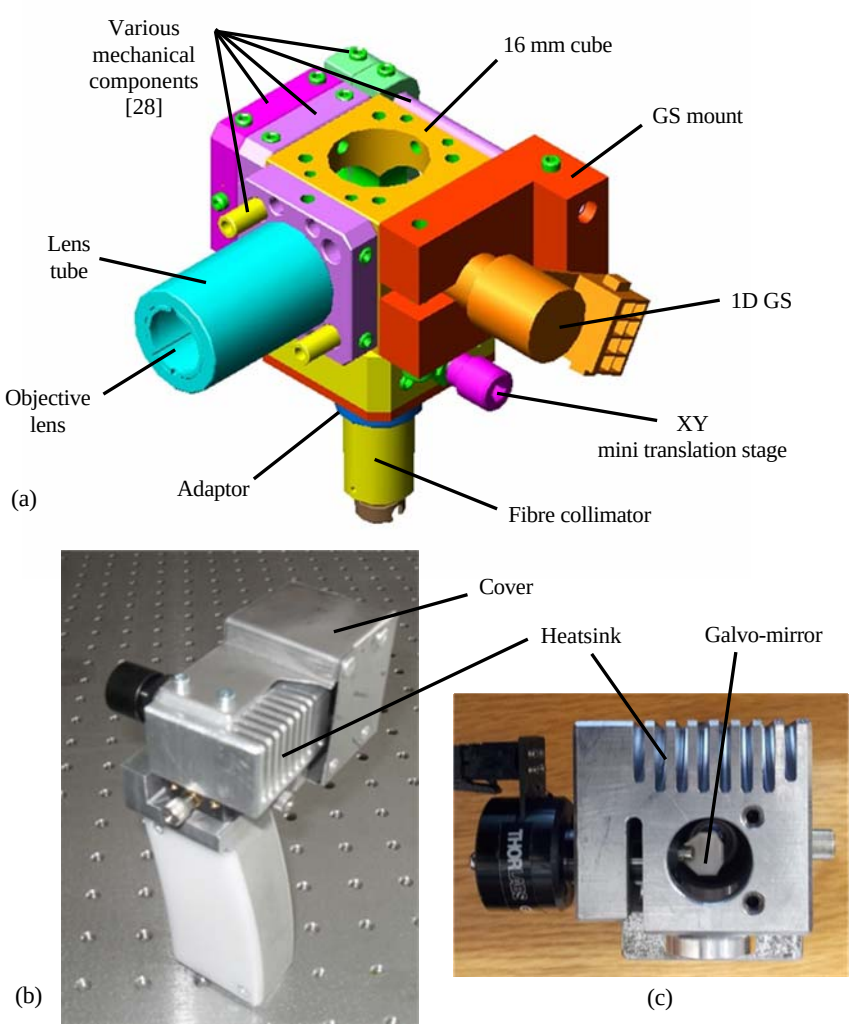

Fig. 2 – Handheld scanning probes with a 1D GS: a) design and components of the core of the first variant (handle not shown); b) second, ergonomic variant (photo of the entire probe); c) photo of (b) from the top, with the cover removed, showing the GS.

Regardless of the probe variant, our option for the scanning device utilized has been the 1D GS, because of its mature technology [29, 30] and of its capability to provide triangular scanning regimes. We have previously demonstrated that

these regimes are optimal in terms of providing the highest duty cycles and the most distortion-free images in comparison to sinusoidal or sawtooth scanning [31, 32]. One has yet to remark that the scan parameters (*i.e.*, scan frequency and amplitude, as well as theoretical duty cycle for sawtooth scan) have to be optimized even for triangular scan – and even more for sawtooth scan [33] – in order to avoid distortions. When such distortions occur, these portions have to be discarded in order to properly collate individual scans to obtain images of larger samples, as we have discussed in detail, developing mathematical models and testing them with different techniques like Fourier Domain (FD) OCT [32] or Gabor Domain Optical Coherence Microscopy (GD-OCM) [33]. Based on our work, other groups achieved such images with other techniques, such as Doppler OCT [34].

In contrast to using GSs, MEMS-based probes with resonant micro-mirrors utilized so far sinusoidal scanning, which for any range of scan parameters for OCT requires post-processing of the signal after image acquisition [25].

However, it is worth mentioning that MEMS with capabilities to provide triangular scan are being developed [35], therefore including such scanning devices in handheld probes is another direction of work in our groups.

4. ELEMENTS OF THE OPTICAL DESIGN

The Thorlabs AC-127-030 achromatic doublet objective lens, placed between the scanning mirror and the sample, focuses the beam at various lateral locations on the sample, acting as a scan lens, with the galvomirror situated in its back focal plane and the sample in its image plane. Our Zemax^{TM} model parameters were: 3 mm beam diameter, working wavelengths of 840 nm and 1330 nm, and an angular field range of 6.6º optical (half range of 3.3º, corresponding to 1.7 mm). We considered both lens orientations: concave-convex, which we denoted “D” (Fig. 3a) and convex-concave, which we denoted “C” (Fig. 3b).

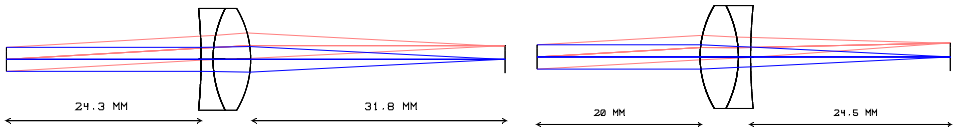

(a) (b)

Fig. 3 – Objective lens in the “D” configuration layout (a) and in the “C” configuration layout (b).

Unsurprisingly in the D configuration the focusing performance of the lens away from the paraxial region suffers considerably. This is seen in the spot diagrams and in the RMS spot radius plot (Fig. 4a), in which a theoretical enlargement of the beam spot from < 5 μm to nearly 30 μm at the edges of the scan

is predicted. Since the Airy radius is 10.1 µm at 840 nm and 16.0 µm at 1330 nm, it is clear that diffraction limited performance is only possible over roughly half of the scan range, *i.e.* just under 2 mm.

There is also an obvious and significant amount of astigmatism as shown by the deviation of the sagittal (S) from the tangential (T) beam components which are separated by about 0.5 mm at the scan edge (field value 3.3 deg) (Fig. 4b). A small amount of coma is also observable in the spot diagrams.

Although the handheld probe was intended to operate initially only at 840 nm and 1330 nm, we have also modelled the longitudinal drift of the focus with wavelength over the intervening range. Fig. 4c shows that a z (longitudinal) shift of 60 µm towards the lens is expected at 1060 nm, although only 10 µm in depth separate the 840 nm and 1330 nm planes of best focus.

In the "C" configuration the RMS spot radius undergoes a smaller change as the beam is scanned across the image plane, to just under 15 µm at the edges of the scan. Given that the Airy radius is now 10.2 µm at 840 nm and 16.1 µm at 1330 nm, we deduce that the lens gives almost diffraction limited performance for 80% of the scan range at 840 nm and for the entire scan range at 1330 nm (Fig. 5a).

Astigmatism is still present but reduced to half as shown by a smaller separation of the sagittal (S) from the tangential (T) beam components, of only about 0.25 mm at the 3.3º field value (Fig. 5b). Coma is however much more evident in the spot diagrams (Fig. 6b). In Fig. 5c the longitudinal shift of the focus with wavelength shows that a 66 µm in depth separate the planes of best focus at 840 nm and 1300 nm.

In conclusion, because of the small angles involved, the lens behaves effectively like an f theta lens and gives in the C configuration diffraction limited performance across our chosen scan range. This allows for a simple approach in the construction of the probe, but places a constraint on its working distance which is set around 25–30 mm. It also limits the achievable field size for diffraction limited performance to 3.4 mm, which is however adequate for the applications we have presented and for numerous others.

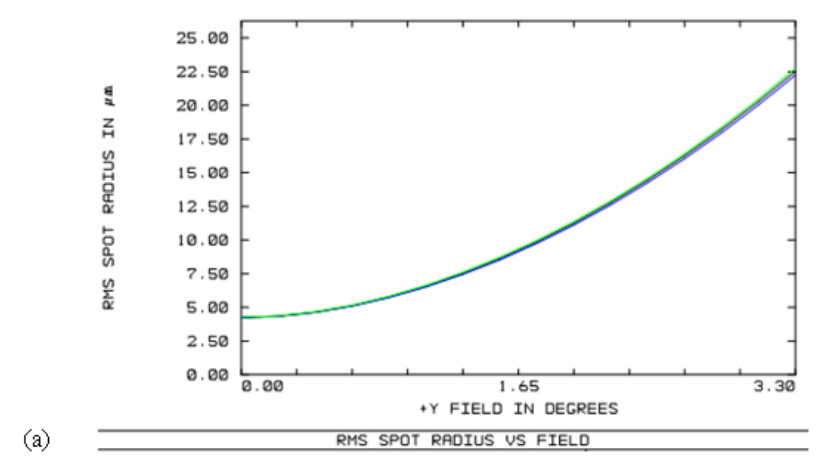

(a)

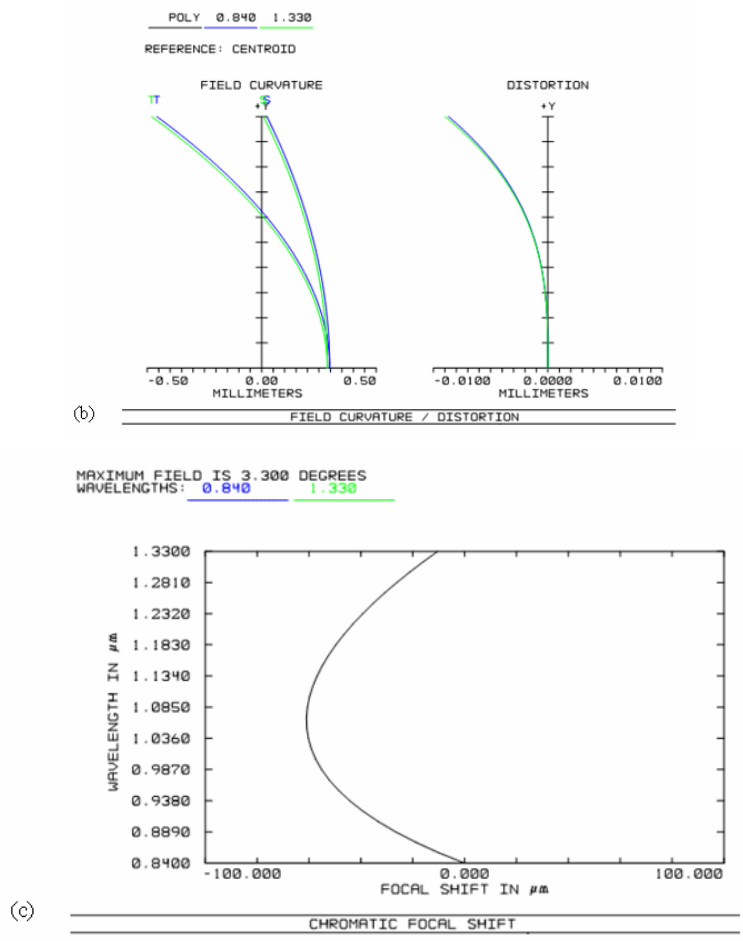

Fig. 4 – Focusing performance of the objective lens in the “D” orientation.

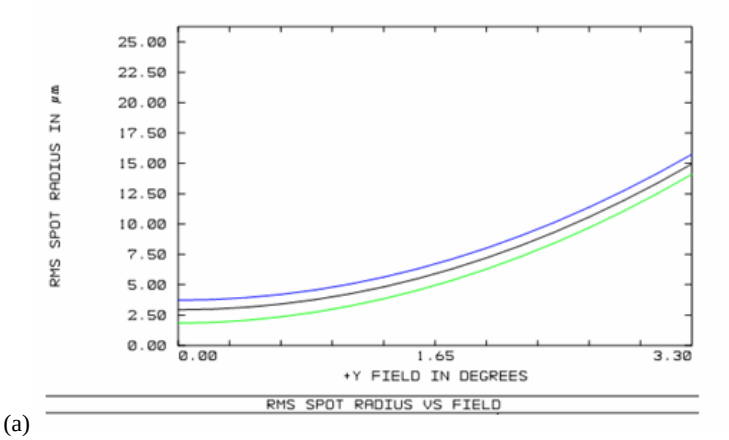

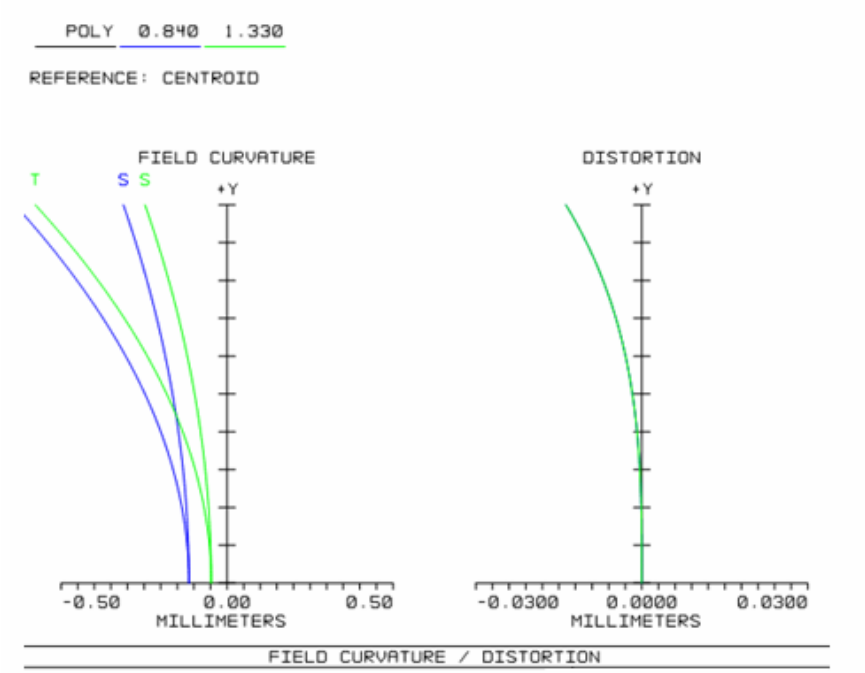

(b)

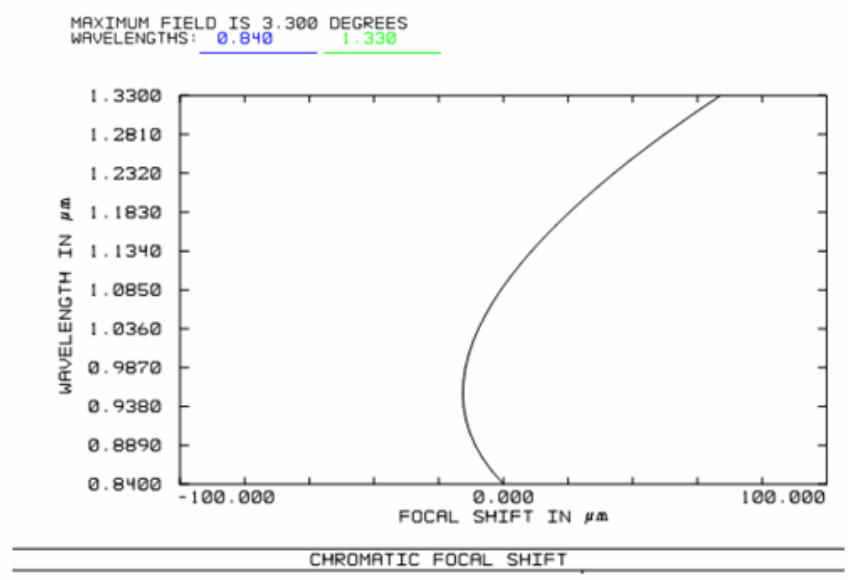

(c)

Fig. 5 – Focusing performance of the objective lens in the “C” orientation.

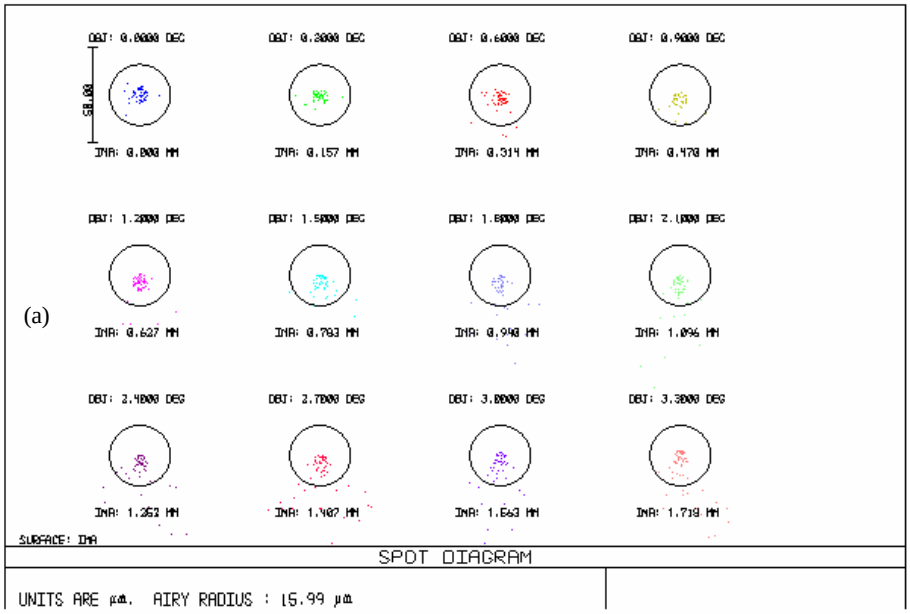

Fig. 6 – Matrix spot diagram for the objective lens in the “D” orientation (a) and in the “C” orientation (b).

5. TESTING OF THE OCT HANDHELD SCANNING PROBE

OCT B-scan images/transversal depth sections obtained with the 1D GS-based handheld probe have been shown in [21] for larynx and vocal cords, as well as in [27] for metalloceramic dental prostheses.

Examples of OCT B-scans taken in our lab with a variant of the probe are shown in Fig. 7 for a plastic card and for paper, as well as for a finger and for a tooth of a healthy volunteer in the group. The anatomic elements of the structure of the skin can be observed (Fig. 7c). The OCT B-scan of a human tooth allows to observe the structure of enamel and dentin (Fig. 7d). The cracks inside the dentin appear as a consequence of an unhealthy habit (bruxism) and could lead to fracture of big pieces of dentin and enamel. If those cracks could be spotted earlier, a specific occlusion treatment would be recommended. Here the OCT technique proves to be a useful non-invasive tool for identify those fractures.

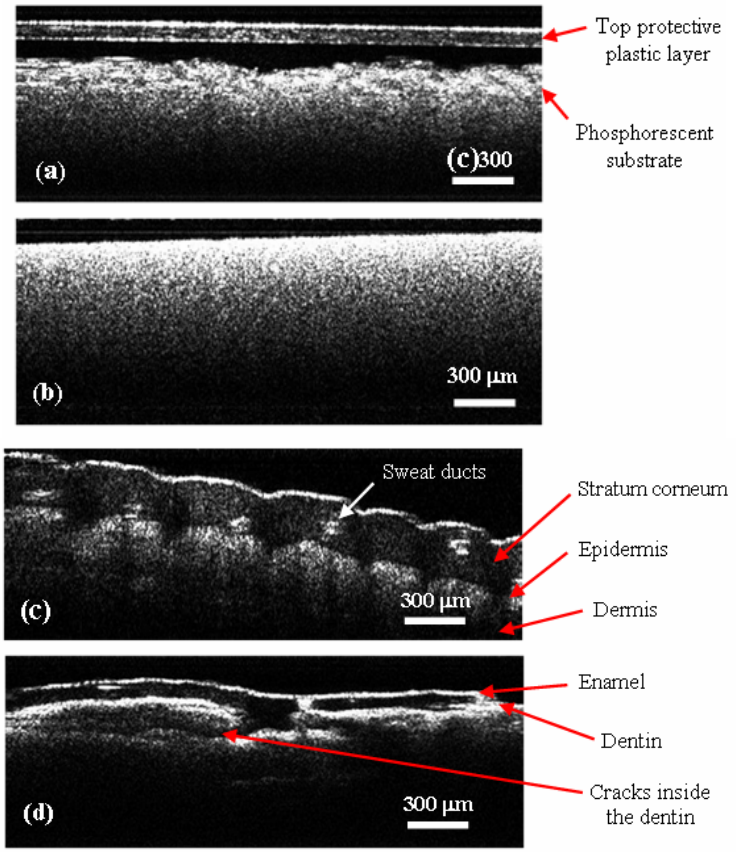

Fig. 7 – Test of the handheld scanning probe for OCT B-scans of: a) an infrared viewing card showing its successive layers; b) 1 mm thick paper; c) a finger; d) a tooth. All the images were obtained with the handheld scanning probe coupled with the SS-OCT system built in-house.

6. CONCLUSIONS

We presented two configurations of 1D GS-based handheld probes for OCT: the first one has been built almost entirely from off-the-shelf components, in order to be made in the lab with a minimum of time and effort, including for educational purposes. The second configuration is an optimized, ergonomic one.

We show in this paper the testing of one of the variants, with the remark that it has been utilized already for ENT investigations at the Northwick Park Hospital (part of London North West Healthcare NHS Trust, London, UK) [21], while another variant of the same probe is being used for dental medicine at the Victor Babes Medicine and Pharmacy University of Timisoara [27]. Here we reported the SS-OCT engine but a variety of SD- and SS-OCT high speed acquisition and display systems have been successfully used with variants of the handheld probe in our groups.

Future work we intend to carry out includes the use of such probes in Non-Destructive Testing (NDT) applications, as we have recently demonstrated in this area that OCT can successfully replace the established but more costly and time consuming method of, Scanning Electron Microscopy (SEM) in the analysis of metallic fractures [36]. Other directions of work include the optimization of the control structure of GSs for an increased precision and speed, while the development of handheld probes with 2D GSs is on-going [24], in order to take advantage of the recently demonstrated master-slave interferometry (MSI) technique [37].

Acknowledgements. This study is supported by a Partnership Grant of the Romanian National Authority for Scientific Research, CNDI–UEFISCDI project number PN-II-PT-PCCA-2011-3.2-1682 (http://3om-group-optomechatronics.ro/). C. Sinescu also acknowledges the partial support of the TE 101/2010 CNDI-UEFISCDI grant. A. Gh. Podoleanu acknowledges the support of ERC 7th Framework Programme, Advanced Grant 'COGATIMABIO'249889, of the NIHR Biomedical Research Centre at Moorfields Eye Hospital NHS Foundation Trust, and of the UCL Institute of Ophthalmology.

REFERENCES

1. D. Huang, E.A. Swanson, C.P. Lin, J.S. Schuman, W.G. Stinson, W. Chang, M.R. Hee, T. Flotte, K. Gregory, C.A. Puliafito, J.G. Fujimoto, Science **254**, *5035*, 1178–1181 (1991).
2. W. Drexler, J.G. Fujimoto, Progress in Retinal and Eye Research **27**, *1*, 45–88 (2008).
3. A. Gh. Podoleanu, J. of Microscopy, **247**, 209–219 (2012).
4. S. Ortiz, P. Pérez-Merino, S. Durán, M. Velasco-Ocana, J. Birkenfeld, A. de Castro, I. Jiménez-Alfaro, S. Marcos, Biomed. Opt. Express **4**, 387–396 (2013).
5. K.-S. Lee, H. Zhao, S.F. Ibrahim, N. Meemon, L. Khoudeir, J.P. Rolland, J. of Biomed. Opt. **17**, *12*, 126006 (2012).
6. F. Feldchtein, V. Gelikonov, R. Iksanov, G. Gelikonov, R. Kuranov, A. Sergeev, N. Gladkova, M. Ourutina, D. Reitze, J. Warren, Opt. Express **3**, 239–250 (1998).

7. C. Sinescu, M.L. Negrutiu, A. Bradu, V.-F. Duma, A. Gh. Podoleanu, Computational and Math. Methods in Medicine, Paper ID 709076 (2015).
8. R. Oancea, A. Bradu, C. Sinescu, R. M. Negru, M.L. Negrutiu, I. Antoniac, V.-F. Duma, A. Gh. Podoleanu, J. of Adhesion Sc. and Techn. **29**, *1*, 49–58 (2015).
9. S. Canjau, C. Todea, C. Sinescu, M. L. Negrutiu, V.-F. Duma, A. Manescu, F. Topala, A. Gh. Podoleanu, Key Eng. Materials **587**, 331–337 (2014).
10. K.H. Kim, B.H. Park, G.N. Maguluri, T.W. Lee, F.J. Rogomentich, M.G. Bancu, B.E. Bouma, J.F. de Boer, J.J. Bernstein, Opt. Express **15**, 18130–18140 (2007).
11. W. Drexler, U. Morgner, F.X. Kärtner, C. Pitris, S.A. Boppart, X.D. Li, E.P. Ippen, J. G. Fujimoto, Opt. Letters **24**, 1221–1223 (1999).
12. W. Wieser, B.R. Biedermann, T. Klein, C.M. Eigenwillig, R. Huber, Opt. Express **18**, *14*, 14685 (2010).
13. M.A. Choma, M. Sarunic, C. Yang, J.A. Izatt, Opt. Express **11**, 2183–2189 (2003).
14. M. Wojtkowski, Applied Optics **49**, D30–D61 (2010).
15. A. Gh. Podoleanu, G.M. Dobre, R.G. Cucu, R. Rosen, P. Garcia, J. Nieto, D. Will, R. Gentile, T. Muldoon, J. Walsh, L.A. Yannuzzi, Y. Fisher, D. Orlock, R. Weitz, J.A. Rogers, S. Dunne, A. Boxer, J. of Biomed. Opt. **9**, 86–93 (2004).
16. A. Gh. Podoleanu, R.B. Rosen, Progress in Retinal and Eye Research **27**, 464–499 (2008).
17. S.A. Boppart, B.E. Bouma, C. Pitris, G.J. Tearney, J.G. Fujimoto, M.E. Brezinski, Opt. Letters **22**, 1618–1620 (1997).
18. A.M. Zysk, F.T. Nguyen, A.L. Oldenburg, D.L. Marks, S.A. Boppart, J. of Biomed. Opt. **12**, *5*, 051403 (2007).
19. S.J. Erickson, A. Godavarty, Med. Eng. Phys. **31**, 495–509 (2009).
20. L.F. Capitán-Vallveya, A.J. Palma, Analytica Chimica Acta **696,** 27–46 (2011).
21. R. Cernat, T.S. Tatla, J. Pang, P.J. Tadrous, A. Bradu, G. Dobre, G. Gelikonov, V. Gelikonov, A. Gh. Podoleanu, Biomed. Opt. Express **3**, *12*, 3346–3356 (2012).
22. W. Jung, J. Kim, M. Jeon, E.J. Chaney, C.N. Stewart, S.A. Boppart, IEEE Trans. on Biomed. Eng. **58**, 741–744 (2011).
23. V.-F. Duma, J. P. Rolland, and A. Gh. Podoleanu, Proc. SPIE **7556**, 7556-10 (2010).
24. V.-F. Duma, Proc. SPIE **8925**, 8925 0L (2014).
25. C.D. Lu, M.F. Kraus, B. Potsaid, J.J. Liu, W. Choi, V. Jayaraman, A.E. Cable, J. Hornegger, J.S. Duke, and J.G. Fujimoto, Biomed. Opt. Express **5**, 293–311 (2014).
26. C. Sinescu, M. L. Negrutiu, V.-F. Duma, C. Marcauteanu, F. I. Topala, M. Rominu, A. Bradu, and A. Gh. Podoleanu, Proc. SPIE **8785**, 8785EH (2013).
27. D. Demian, V.-F. Duma, C. Sinescu, M.L. Negrutiu, R. Cernat, F.I. Topala, Gh. Hutiu, A. Bradu, A. Gh. Podoleanu, J. of Eng. in Medicine **228**, *8*, 743–753 (2014).
28. http://optovue.com/
29. G. F. Marshall, *Handbook of Optical and Laser Scanning*, CRC Press, New York, 2011.
30. J. Montagu, Encyclopedia of Optical Engineering, 2465–2487 (2003), DOI: 10.1081/E-EOE-120009595.
31. V.-F. Duma, Opt. Eng. **49**, *10*, 103001 (2010).
32. V.-F. Duma, K.-S. Lee, P. Meemon, J.P. Rolland, Appl. Opt. **50**, 5735–5749 (2011).
33. V.-F. Duma, P. Tankam, J. Huang, J.J. Won, J.P. Rolland, Appl. Opt. **54**, *17*, 5495–5507 (2015).
34. B. Braaf, K.A. Vermeer, K.V. Vienola, and J.F. de Boer, Opt. Express **20**, *18*, 20516–20534 (2012).
35. http://mirrorcletech.com/
36. Gh. Hutiu, V.-F. Duma, D. Demian, A. Bradu, and A. Gh. Podoleanu, Appl. Opt. **53**, *26*, 5912–5916 (2014).
37. A. Gh. Podoleanu and A. Bradu, Opt. Express **21**, 19324–19338 (2013).